Table of Contents

Experimental Section

The preparation of $NiMoO_4$ precursor: Typically, a commercial nickel foam (NF; 5 × 30 mm; thickness 1.6mm; porosity 95%) was sonicated with acetone for 30 min, then washed by ethanol and water for several time. After that, the NF was put into a 10 wt % HCl solution for 30 min to clean the surface oxide layer. And then, the NF was washed with water and acetone for several times and dried under N_2 gas. Next, one piece of NF was immersed into 20 mL of H_2O containing 1 mmol $NiCl_2$ and 1 mmol Na_2MoO_4 in a Teflon autoclave. After continuous stirring for 30 min, the autoclave was put into a muffle furnace and heated at 160 ^oC for 6 h. After the autoclave was cooling to room temperature, the $NiMoO_4$/NF was taken out and washed with deionized water for several times.

The preparation of NiMo-based catalysts: In a typical process, the above synthesized $NiMoO_4$ precursor was put into a tube furnace and heated at different temperature (450 ^oC, 500 ^oC, 550 ^oC and 600 ^oC) in a mixed H_2/NH_3 (5% H_2) atmosphere for 2 h. Then, the as-prepared NiMo-H_2/NH_3 catalysts were immersed by ethanol before taking out and kept under N_2 gas for characterization. The NiMo-NH_3 and NiMo-H_2 catalysts were prepared following the same procedures, except for changing the atmosphere into pure NH_3 or mixed H_2/N_2 (5% H_2) gas.

The preparation of Fe-NiMo-based catalysts: For the growth of FeOOH nanoclusters onto NiMo-based electrodes, the above synthesized NiMo-H_2/NH_3**,** NiMo-NH_3 and NiMo-H_2/N_2 electrodes were dipped into 25 ml of a freshly prepared $FeCl_3$ solution (1 mmol) for 15 min under continuous stirring. After that, the electrodes were taken out and put into oven for drying at 70 ^oC. After drying in air for 1 h, the Fe-NiMo-based catalysts were ready for anodic activation and further electrochemical tests.

The preparation of NiMo-based and Fe-NiMo-based powders: Typically, 50 mg $NiMoO_4$ powder was put into a tube furnace and heated at 550 ^oC in mixed H_2/N_2, NH_3/H_2 and pure NH_3 gas for 2h, respectively. The products were taken out after the samples were cooling to room temperature. Next, 10 mg of NiMo-H_2/NH_3**,** NiMo-NH_3 and NiMo-H_2/N_2 powder was added into 2 ml of 0.01 M $FeCl_3$ ethanol solution, respectively. After sonicating for 1h, the above solutions were put into oven for drying at 70 ^oC. The Fe-NiMo-based ready for anodic activation and further electrochemical tests after drying in air for 5 h.

Characterization: TEM measurement was carried out on a FEI Tecnai Osiris electron microscope equipped with a high-brightness field emission gun (XFEG) and an energy dispersive X-ray spectroscopy (EDX) analyzer. XPS measurements were performed on a PHI5000 Versa Probe II XPS system by Physical Electronics (PHI) with a detection limit of 1 atomic percent. Monochromatic X-rays were generated by an Al Kα source (1,4867 eV). The diameter of the analyzed area is 10 μm. The contact angles were taken from contact angle measuring instrument DSA 100 at room temperature. Electrochemical active surface area (ECSA) was calculated by the electrochemical double-layer capacitance. The C_{dl} and C_s are the double-layer capacitance of the working electrodes and a flat $NiFeO_x$ (0.081 mF cm^{-2}) for OER, respectively. The equation is ECSA= C_{dl}/C_s. The calculation of TOF was according to the equations: $TOF = \frac{J \times A}{4 \times F \times m}$, where J is the current density at a given overpotential, A is the geometric surface area of the electrode, F is the Faraday constant (a value of 96485 C mol^{-1}), and m is the number of active site on the electrode. The Fe loadings are measured by ICP-OES. The total amount of Fe-Ni unit is identical to the amount of Fe ions. Thus, m can be represented by the total number of Fe ions.

Electrochemical Measurements: All the electrochemical tests were carried out on a multichannel potentiostat/galvanostat (VSP, Bio-Logic) electrochemical workstation using a three-electrode system. A saturated Ag/AgCl (saturated KCl solution) was used as the reference electrode (RE) and a 1 M KOH solution was used as the electrolyte. The Fe-NiMo-based and NiMo-based catalysts on NF were used as working electrodes directly. The linear sweeping voltammetry (LSV) scans were recorded at a scan rate of 1 mV s^{-1}. The potential range is from 0 V to 0.6 V versus Ag/AgCl for OER. Ohmic drop correction was performed using the current interrupt (CI) method available in the potentiostat software. Chronopotentiometric measurements were carried out to evaluate the long-term stability. Electrochemical impedance spectroscopy (EIS) measurements were carried out by applying an AC voltage with 5 mV amplitude in a frequency range from 100 KHz to 10 mHz. All of the potentials were calibrated to the reversible hydrogen electrode (RHE) according to Nernst equation.

The assembly and performance test of MEAs: The NiMo-based and Fe-NiMo-based powders were first ground in a mortar for uniformity. Then, 5 mg of each sample powders was mixed with 40 ul

Nafion solution (as binder) and 1 ml ethanol. The mixed solution was subjected to ultrasonication for 1 h to obtain a highly disperse catalyst ink. The ink was immediately spray onto carbon paper. The loading mass of catalyst was about 3.0 mg cm^{-2}. The NiMo-based catalysts were used as cathode layers and Fe-NiMo-based catalysts were used as anode layers. Subsequently, cathode and anode were sandwiched with a sustainion anion exchange membrane (X37-50 grade T, Dioxide Materials) and pressed to prepare a membrane electrode assembly (MEA) device. The flowing 1 M KOH solution was used as electrolyte and the temperature of electrolyte can be controlled at 20 °C to 80 °C by a constant temperature heating chamber. The potential range is from 1.1 V to 1.8 V at a scan rate of 1 mV s^{-1}. The corresponding energy conversion efficiency was calculated according to the following equations: 1) $\eta = E_0/V$; 2) $E_0 = -\Delta G/nF$; 3) $\Delta G=\Delta H-T\Delta S$, where η is the energy conversion efficiency and E_0 is the theoretical voltage of water splitting ($H_2O \rightarrow H_2 + 1/2O_2$). n is the number of electrons, F is the Faradaic constant (96485 C mol^{-1}), T is the reaction temperature and V is the measured voltage. ΔG is the change of Gibbs free energy, ΔH is the change of enthalpy (-285.8 kJ mol^{-1}) and ΔS is the change of entropy (-163.34 J K^{-1} mol^{-1}) during water electrolysis.

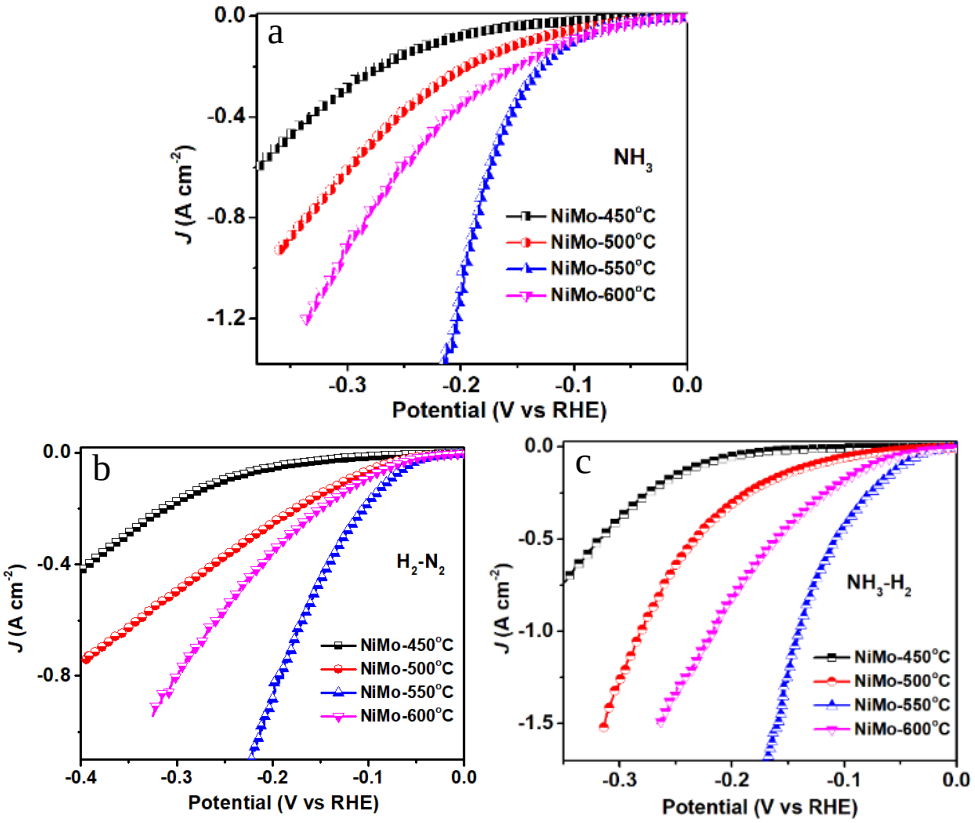

Figure S1 Polarization curves of a) NiMo-NH_3, b) NiMo-N_2/H_2, and c) NiMo-NH_3/H_2 samples that were synthesized at different temperatures for HER in 1 M KOH.

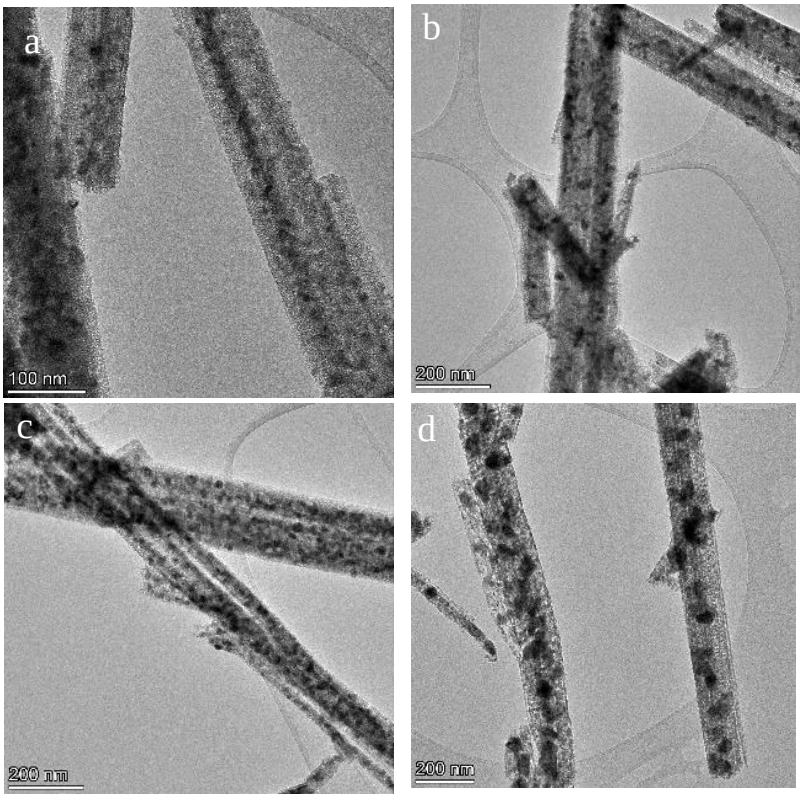

Figure S2 TEM images of NiMo-H_2/N_2 catalysts synthesized at a temperature of a) 450 ºC, b) 500 ºC, c) 550 ºC and d) 600 ºC.

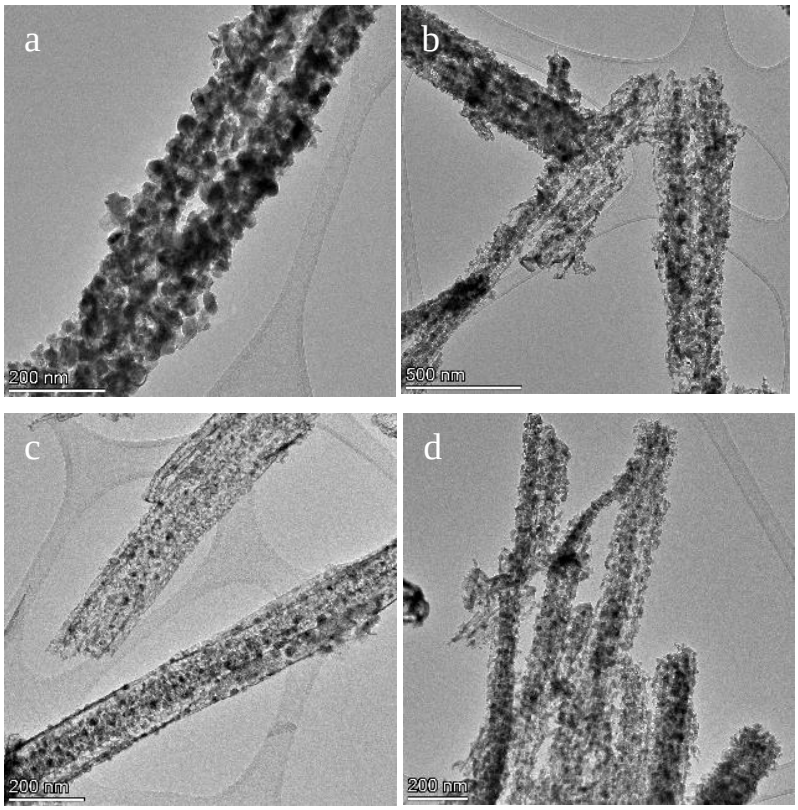

Figure S3 TEM images of NiMo-NH_3 catalysts synthesized at a temperature of a) 450 ^oC, b) 500 ^oC, c) 550 ^oC and d) 600 ^oC.

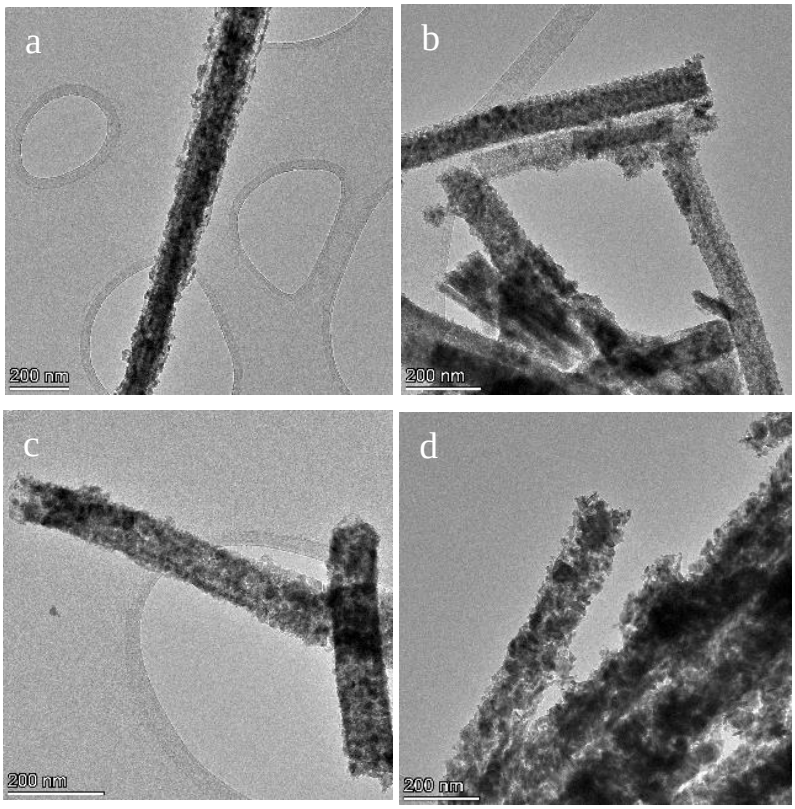

Figure S4 TEM images of NiMo-H_2/NH_3 catalysts synthesized at a temperature of a) 450 ^oC, b) 500 ^oC, c) 550 ^oC and d) 600 ^oC.

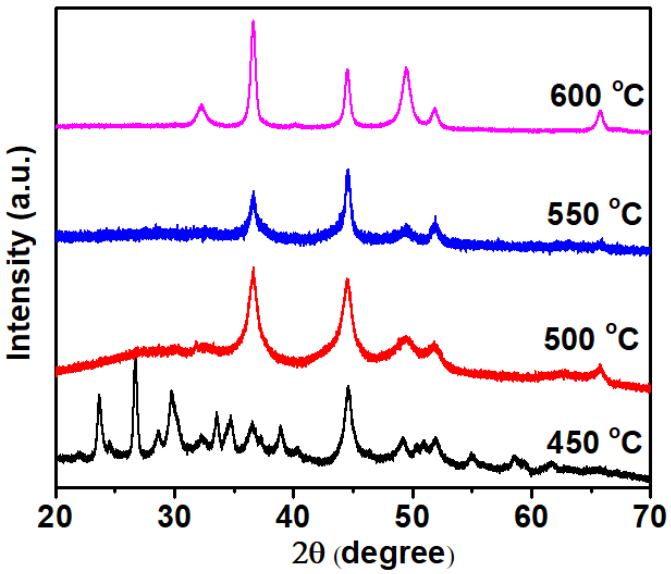

Figure S5 The XRD patterns of NiMo-NH_3/H_2 catalysts synthesized at different reaction temperatures.

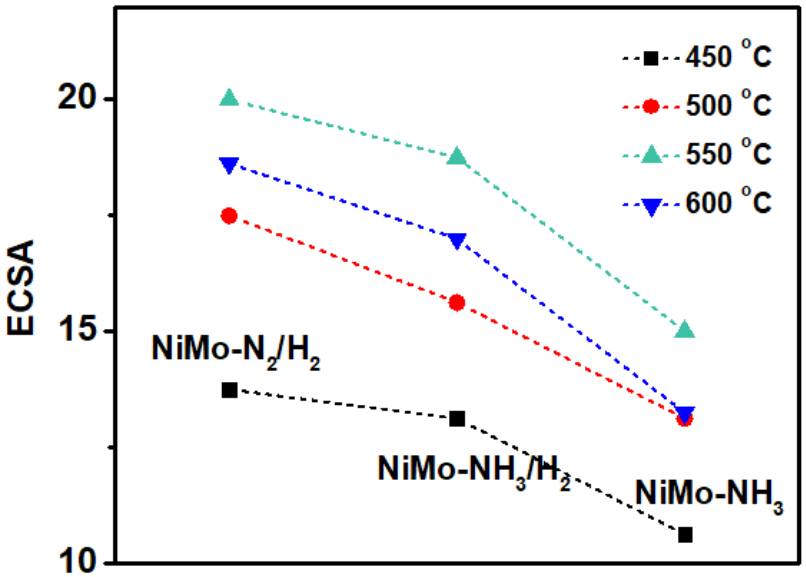

Figure S6 The ECSA values of NiMo catalysts synthesized at different temperatures and under different gases.

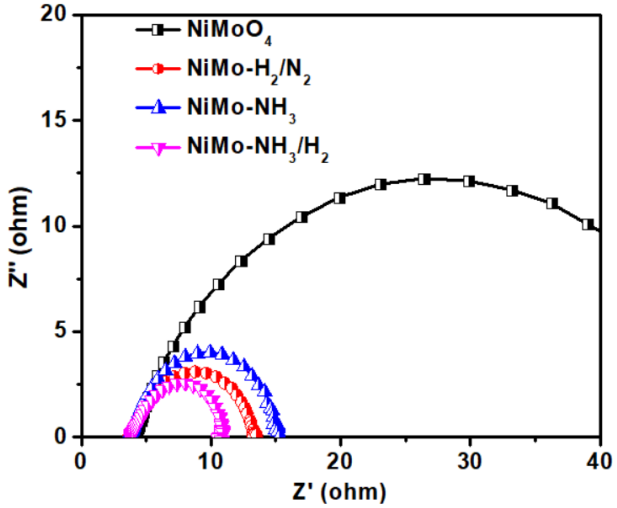

Figure S7 The EIS spectraof different NiMo-based catalysts at -0.1 V for HER.

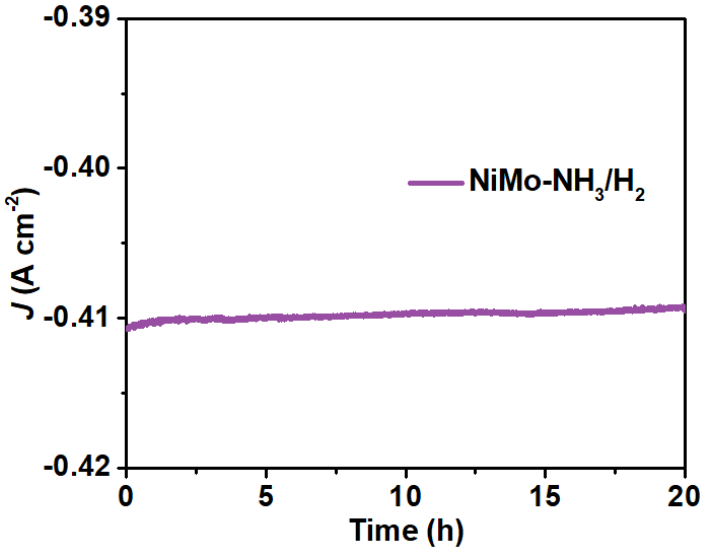

Figure S8 Chronopotentiometric measurement of HER at the potential of -0.1 V using NiMo-NH_3/H_2 as catalyst.

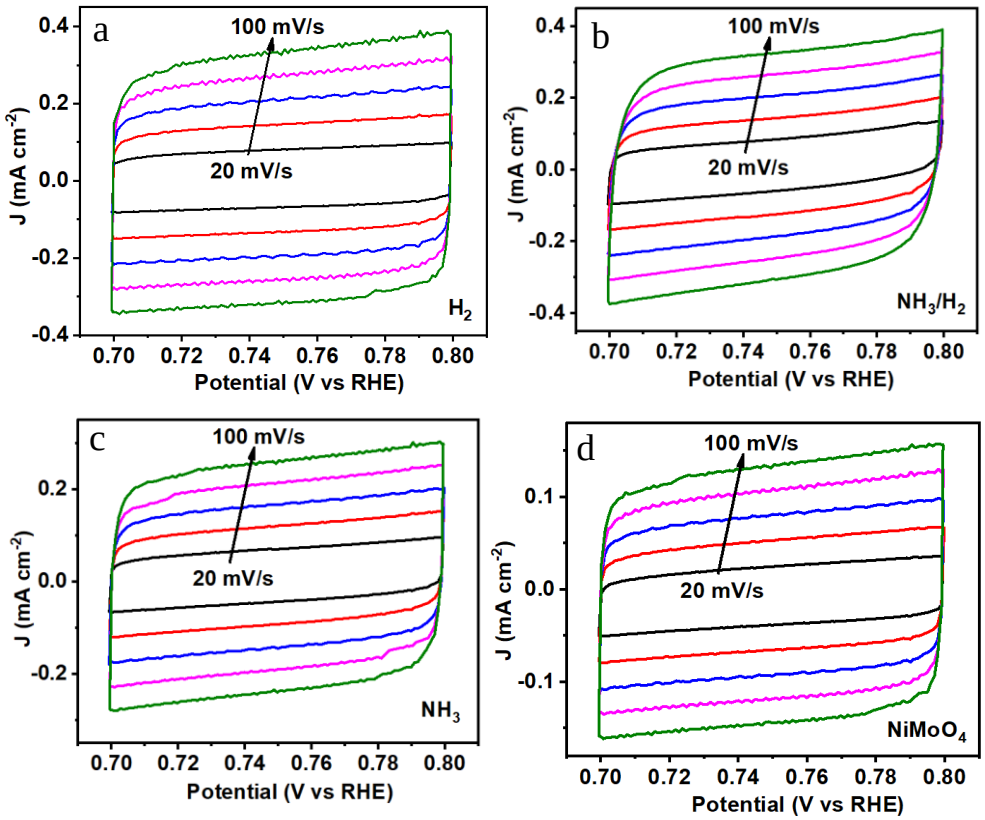

Figure S9 The double-layer capacitances. The CV curves of a) NiMo-N_2/H_2, b) NiMo-NH_3/H_2, c) NiMo-NH_3 and d) pristine $NiMoO_4$ electrodes in 1.0 M KOH at scan rates from 20 to 100 $mV\cdot s^{-1}$.

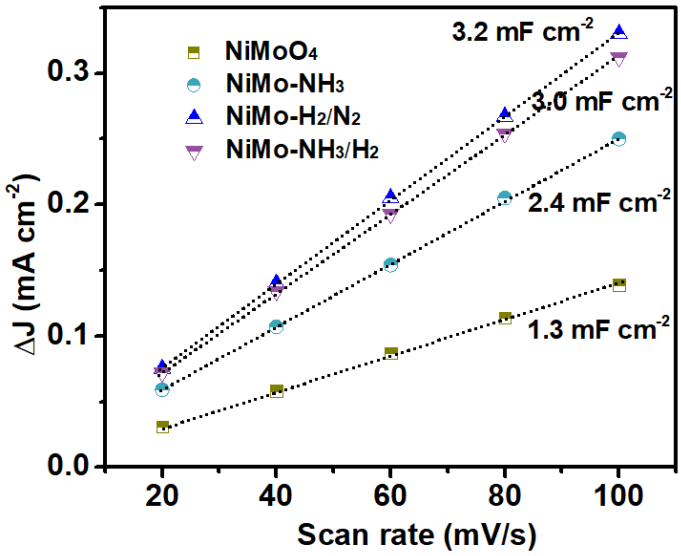

Figure S10 Plots for calculating C_{dl} of NiMo-NH_3/H_2, NiMo-N_2/H_2, NiMo-NH_3 and $NiMoO_4$ electrodes. Scan rate: 20 mV s^{-1} to 100 mV s^{-1}; Potential: 0.7 V to 0.8 V vs RHE.

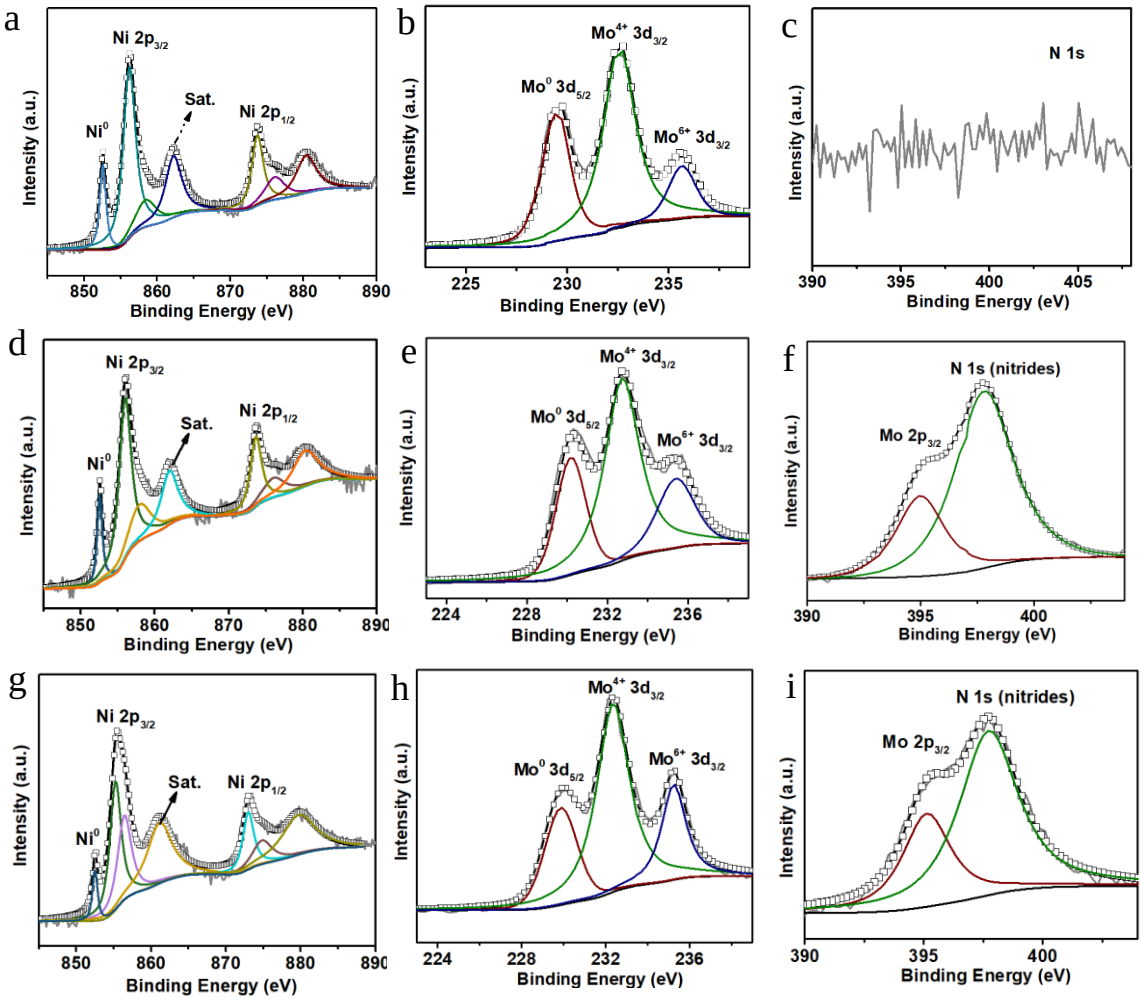

Figure S11 The XPS spectra of NiMo-based materials. (a-c) High-resolution of Ni 2p, Mo 3d and N 1s for NiMo-N_2/H_2. (d-f) High-resolution of Ni 2p, Mo 3d and N 1s for NiMo-NH_3/H_2. (g-i) High-resolution of Ni 2p, Mo 3d and N 1s for NiMo-NH_3.

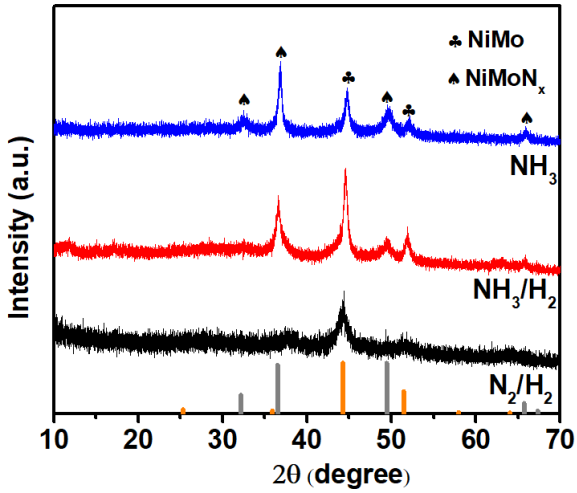

Figure S12 The XRD patterns of NiMo catalysts synthesized at 550 °C.

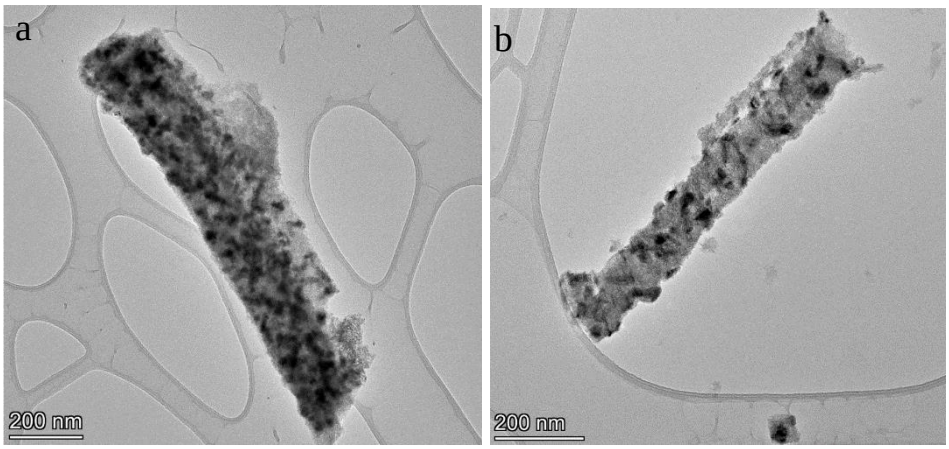

Figure S13 TEM images of Fe-NiMo-N_2/H_2 and Fe-NiMo-NH_3 catalysts detached from nickel foam support.

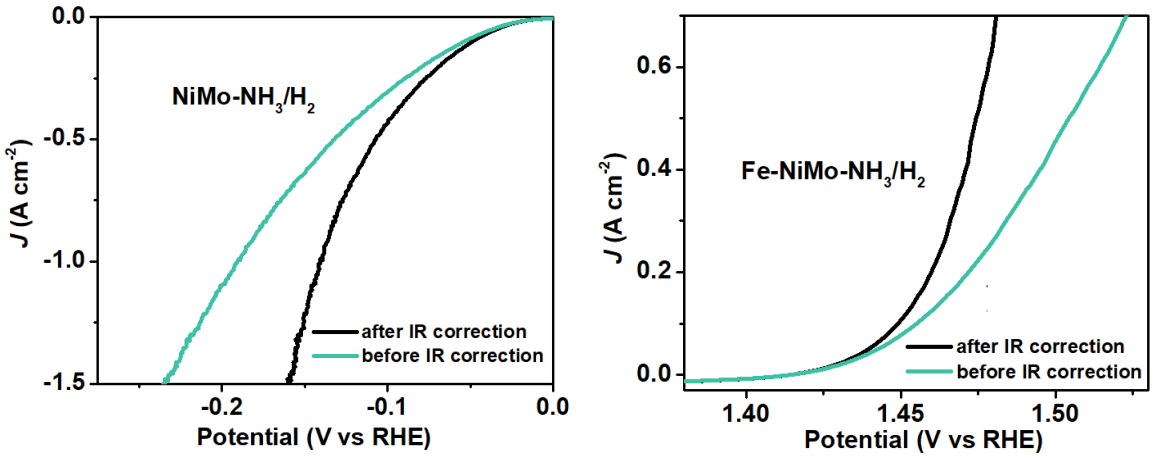

Figure S14 a) The original and IR-corrected LSV curve of NiMo-NH_3/H_2 catalyst for HER. b) The original and IR-corrected LSV curve of Fe-NiMo-NH_3/H_2 catalyst for OER.

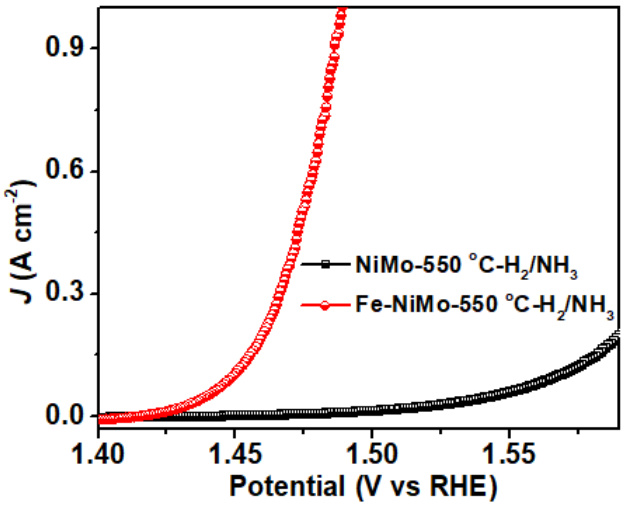

Figure S15 Polarization curves of NiMo-NH_3/H_2 and Fe-NiMo-NH_3/H_2 catalysts for OER in 1 M KOH; scan rate: 1 mV/s.

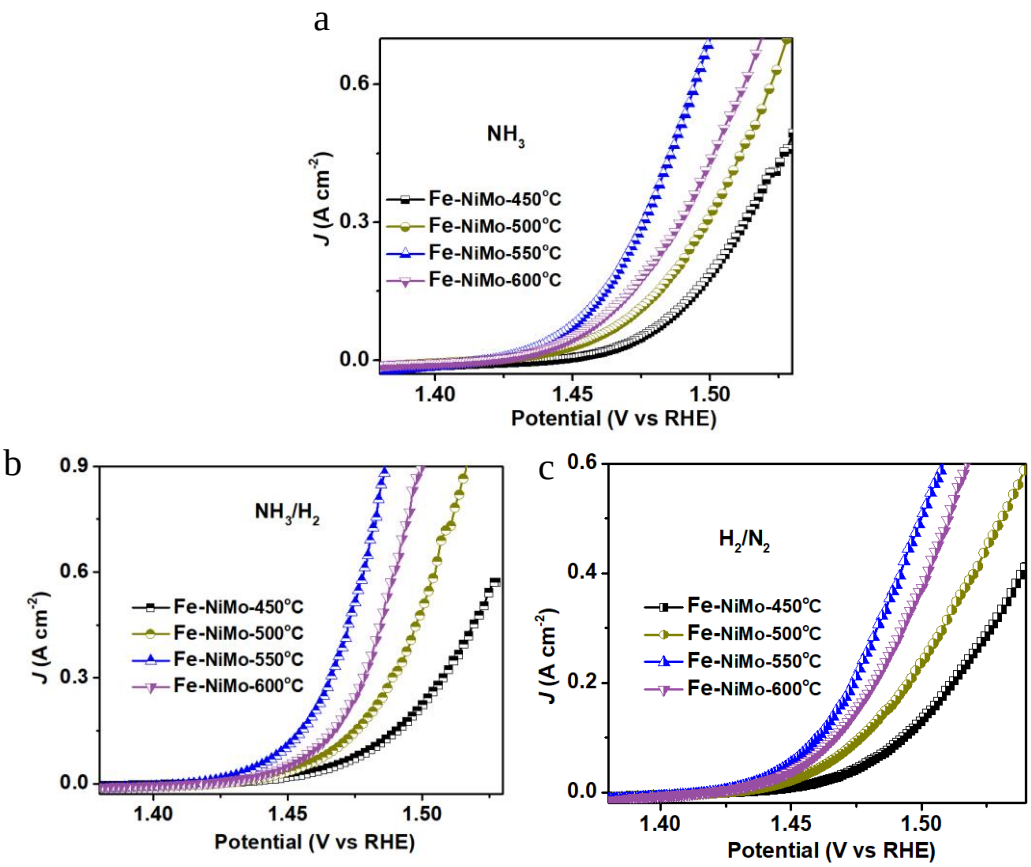

Figure S16 Polarization curves of a) Fe-NiMo-NH_3, b) Fe-NiMo-NH_3/H_2, and c) Fe-NiMo-N_2/H_2 synthesized at different temperatures for OER in 1 M KOH; scan rate: 1 mV/s.

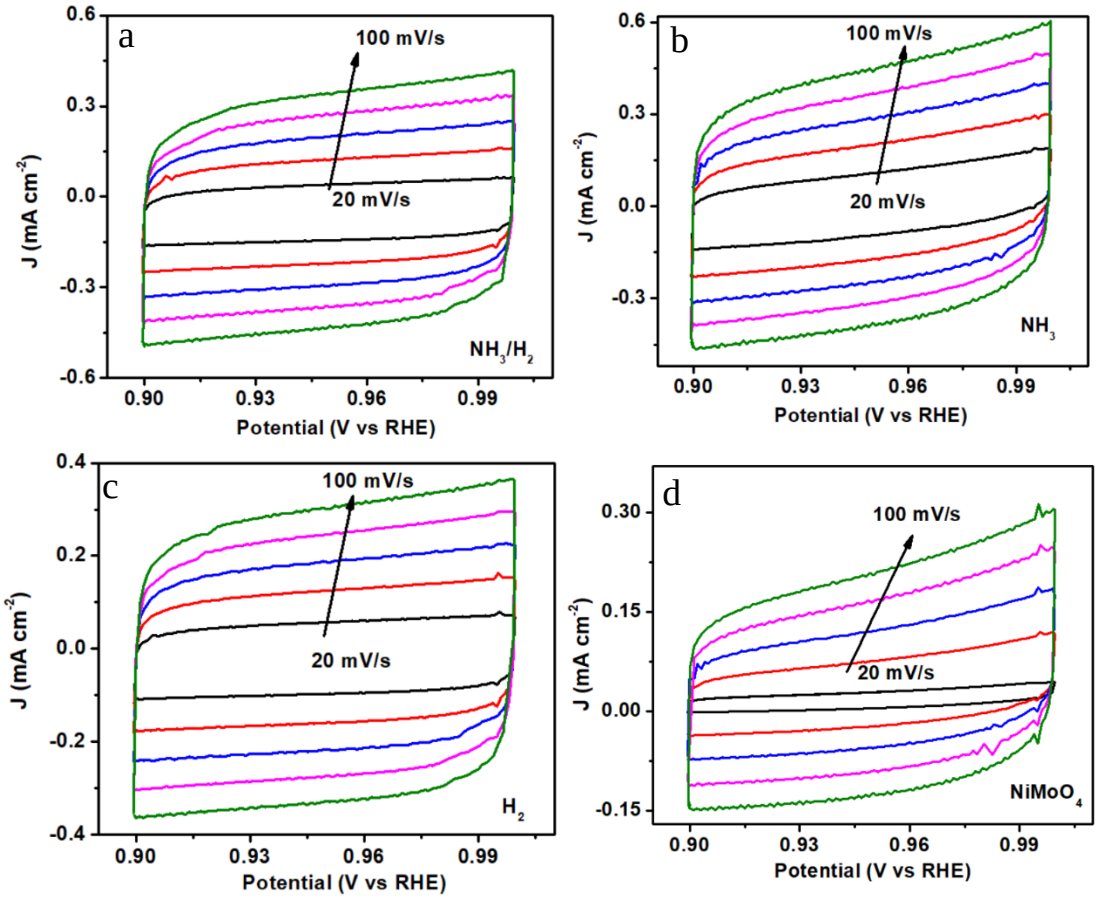

Figure S17 The double-layer capacitances. The CV curves of a) Fe-NiMo-NH_3/H_2, b) Fe-NiMo-NH_3, c) Fe-NiMo-N_2/H_2 and d) pristine Fe-$NiMoO_4$ electrodes in 1.0 M KOH at scan rates from 20 to 100 mV· s^{-1}.

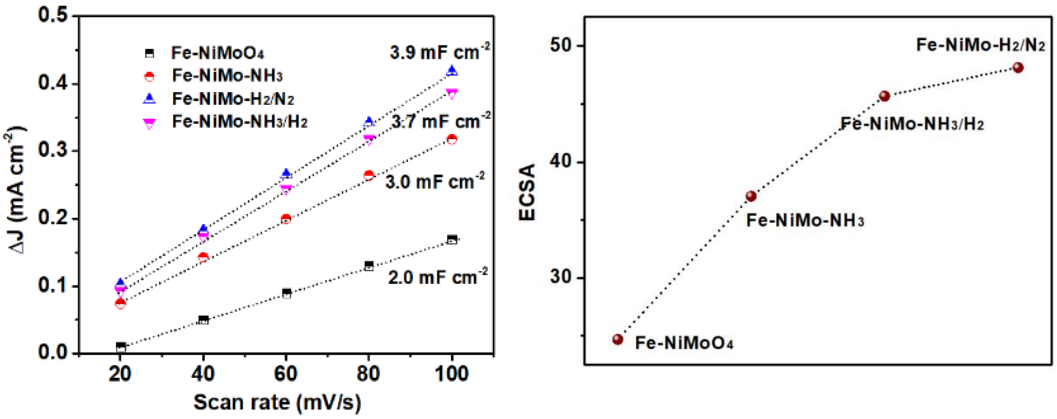

Figure S18 The Plots for calculating C_{dl} and ECSAs of Fe-NiMo-NH_3/H_2, Fe-NiMo-N_2/H_2, Fe-NiMo-NH_3 and Fe-$NiMoO_4$.

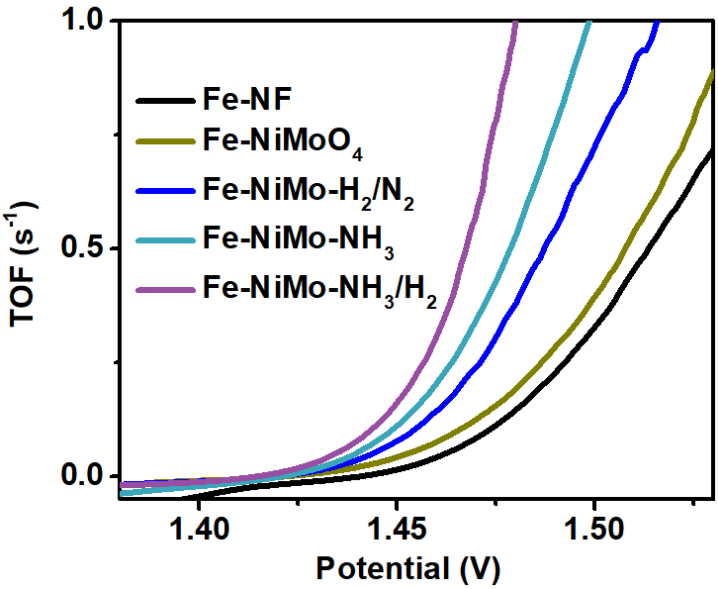

Figure S19 The TOF curves of different Fe-NiMo-based electrodes at different potentials.

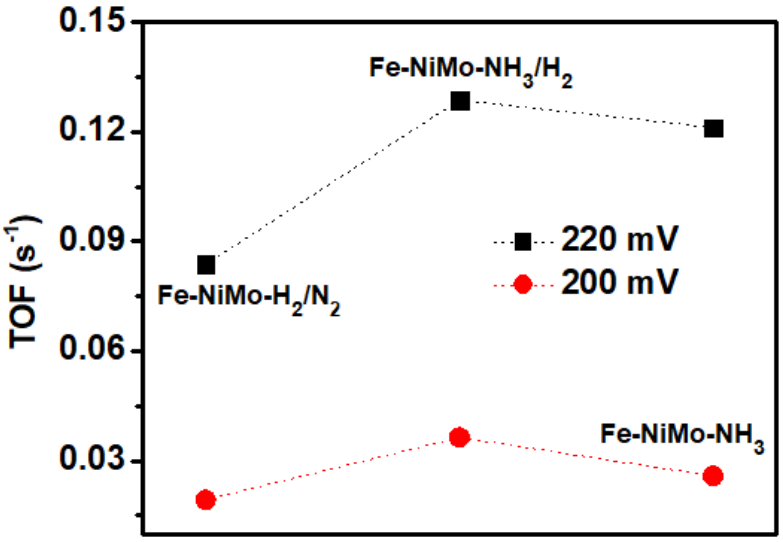

Figure S20 The TOFs of Fe-NiMo catalysts loaded on a carbon cloth support.

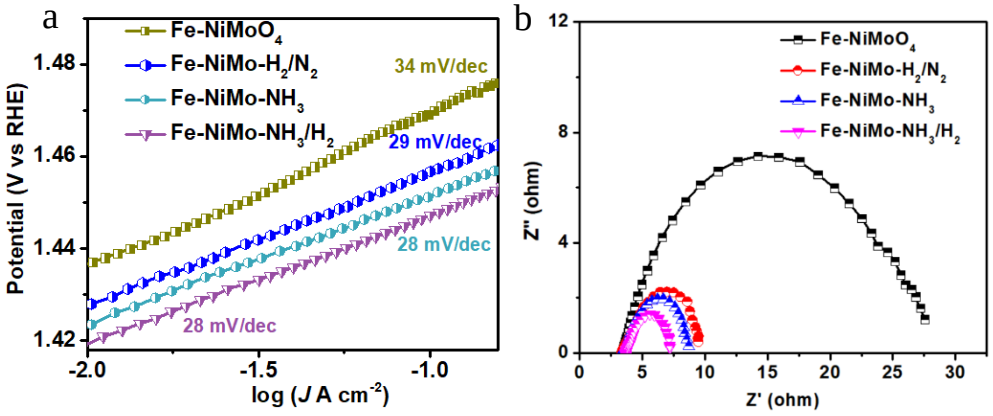

Figure S21 The a) Tafel slopes and b) EIS spectra of Fe-NiMo-NH_3/H_2, Fe-NiMo-N_2/H_2, Fe-NiMo-NH_3 and Fe-$NiMoO_4$ electrodes at 1.45 V for OER.

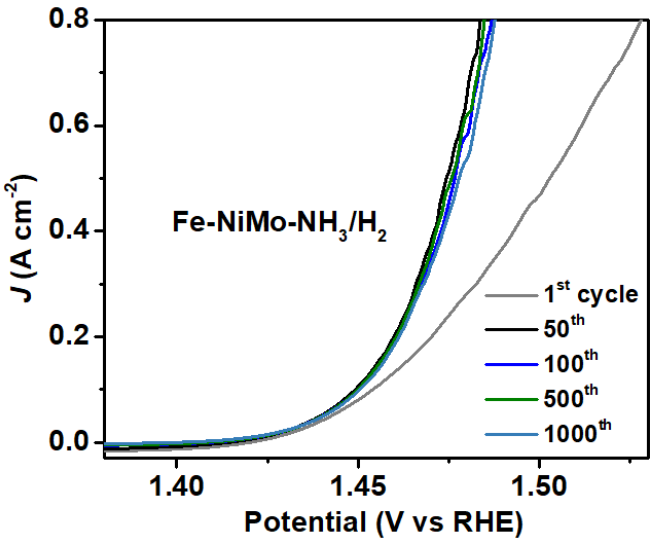

Figure S22 The IR-corrected polarization curves of Fe-NiMo-NH_3/H_2 catalyst after different CV cycles in 1 M KOH solution.

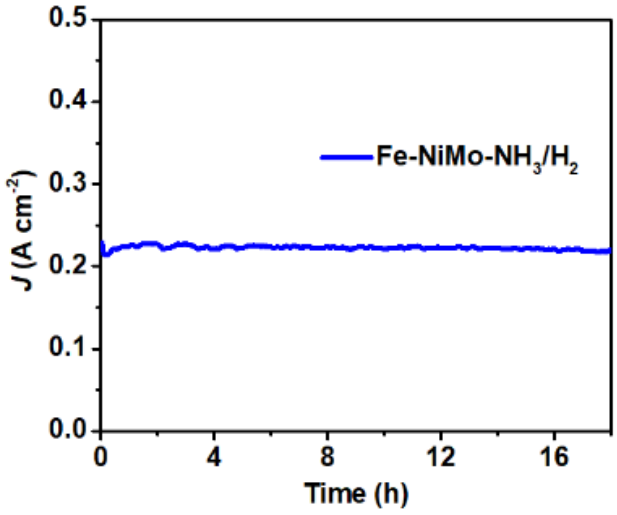

Figure S23 Chronopotentiometric measurement of OER at the potential of 1.46 V using Fe-NiMo-NH_3/H_2 as catalyst.

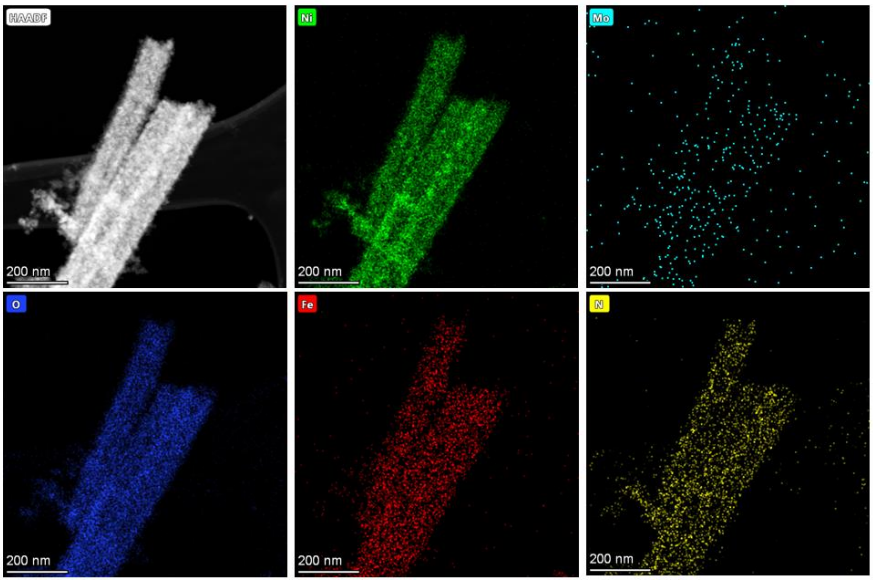

Figure S24 The corresponding element mapping images of Fe-NiMo-NH_3 catalyst detached from NF support after anodic activation.

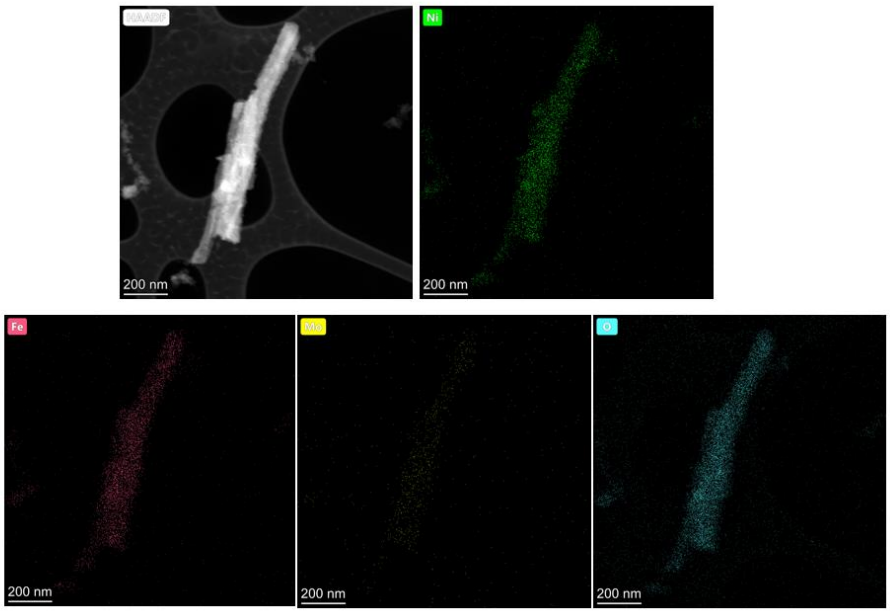

Figure S25 The corresponding element mapping images of Fe-NiMo-H_2/N_2 catalyst detached NF support after anodic activation.

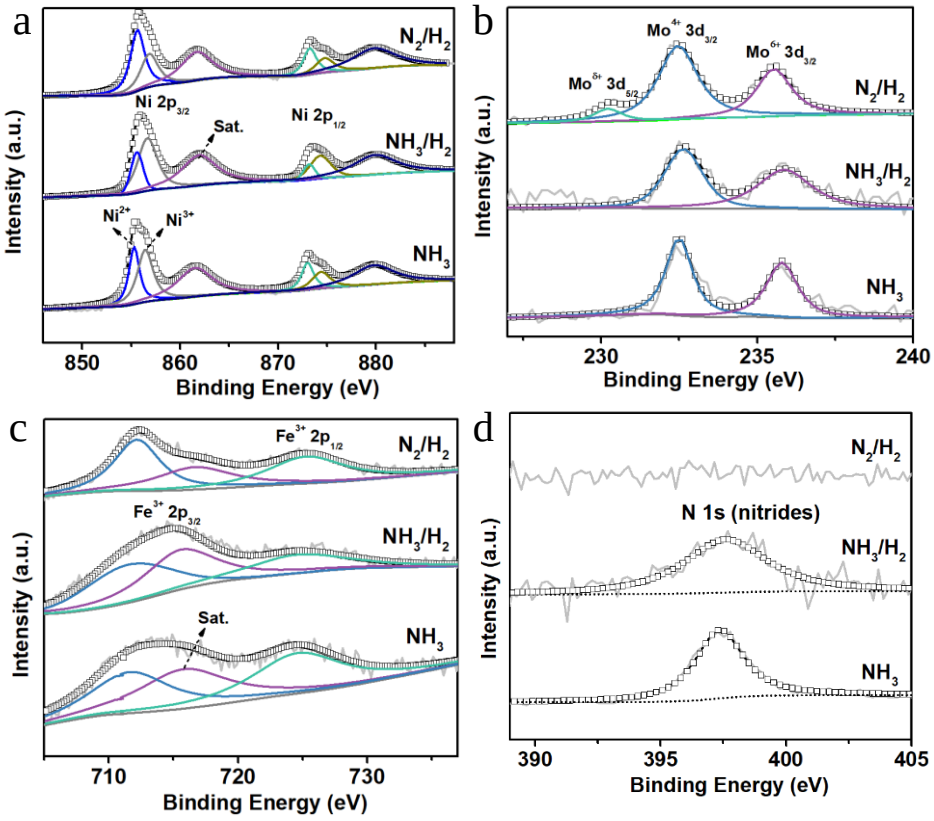

Figure S26 The XPS spectra of Fe modified NiMo samples after anodic activation. High-resolution spectra of (a) Ni 2p, (b) Mo 3d, (c) Fe 2p and (d) N 1s for Fe-NiMo-N_2/H_2, NiMo-NH_3/H_2 and Fe-NiMo-NH_3 catalysts.

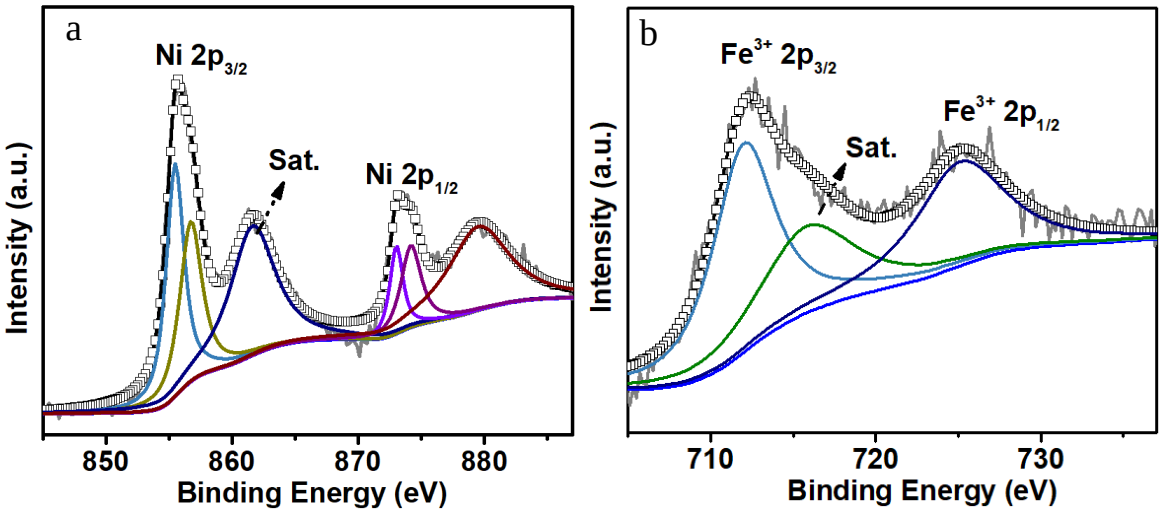

Figure S27 The XPS spectra of Fe-NiO_x-NF electrodes after anodic activation. High-resolution spectra of (a) Ni 2p and (b) Fe 2p.

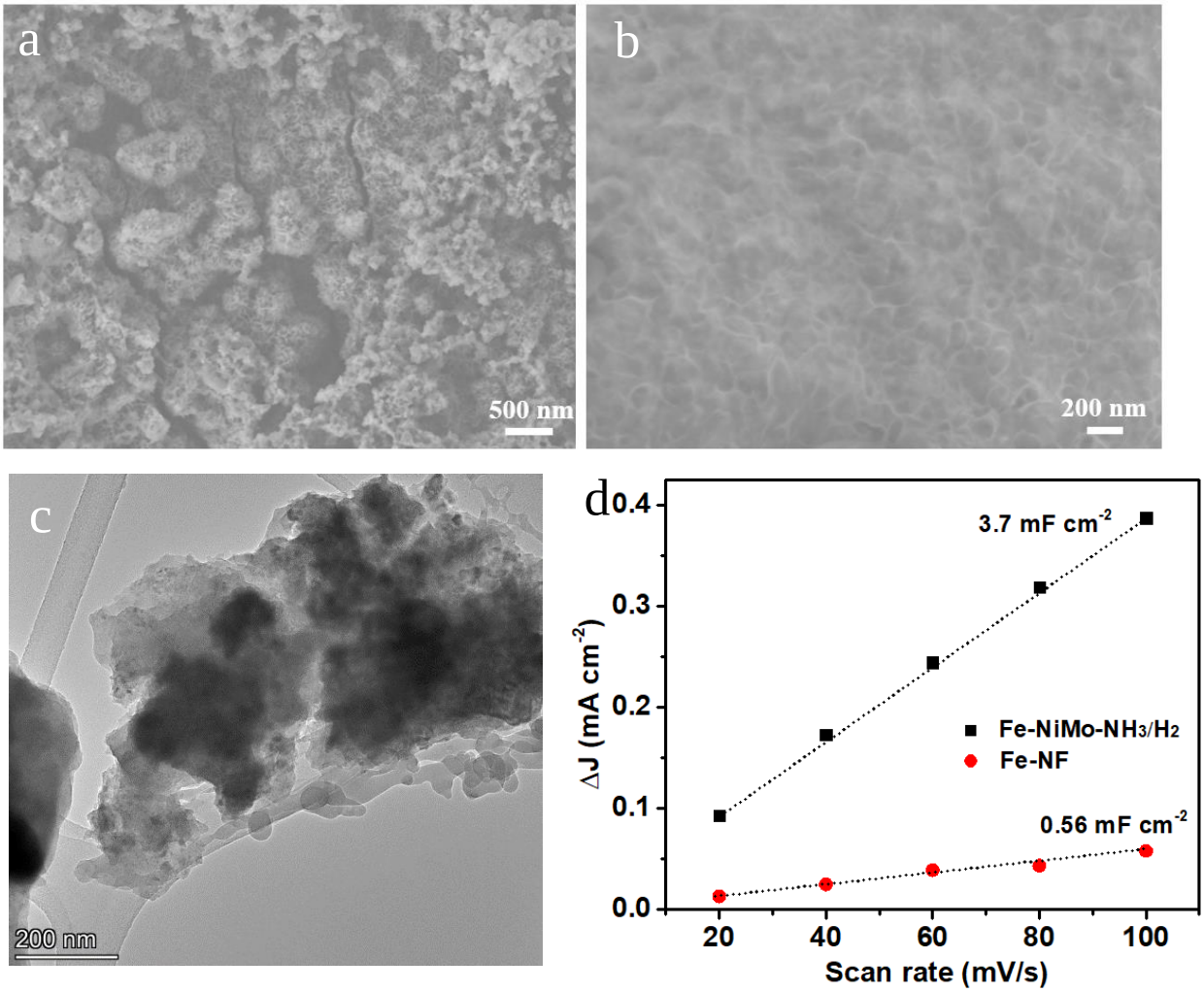

Figure S28 The SEM images of a) Fe-NiMo-NH_3/H_2 and b) Fe-NiO_x-NF electrodes after anodic activation. c) The TEM image of Fe-NiO_x-NF catalyst that detached from nickel foam. d) The plots for calculating C_{dl} of NiMo-NH_3/H_2 and Fe-NiO_x-NF electrodes. Scan rate: 20 mV s^{-1} to 100 mV s^{-1}.

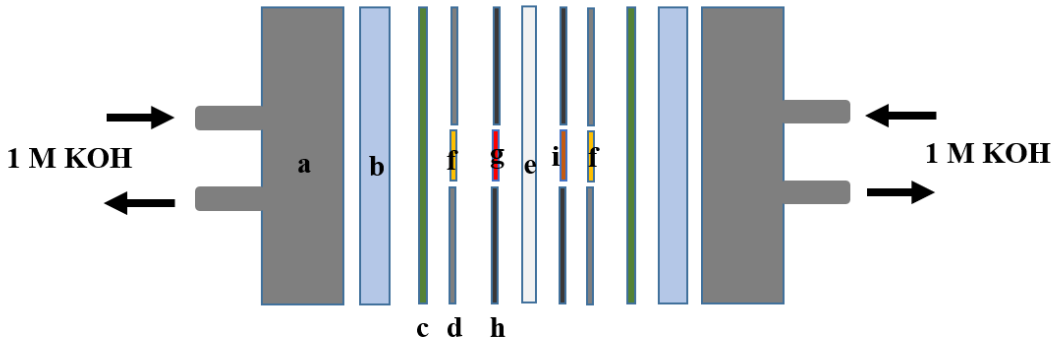

a : Stainless steel support with the inlet and outlet of KOH solution

b : Polytetrafluoroethylene layer (PTFE)

c: Gasket for preventing the leakage

d: Conductive plate

e: Sustainion anion exchange membrane

f: Nickel foam supporter

g: Cathode catalyst layer on carbon paper

i: Anode catalyst layer on carbon paper

h: PET insulative plate

Figure S29 The schematic illustration of a MEA for water electrolysis.

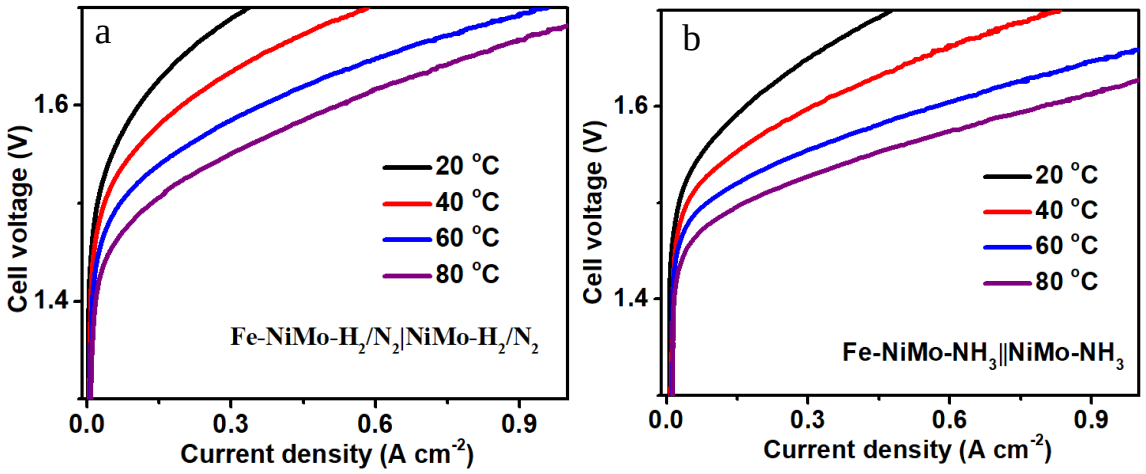

Figure S30 The performance of MEAs employing Fe-NiMo-N_2/H_2||NiMo-N_2/H_2 and Fe-NiMo-NH_3 ||NiMo-NH_3 pairs at temperatures from 20 °C to 80 °C.

Table S1. The C_{dl} and ECSA values of NiMo-based materials.

	Catalysts			
	NiMo-N_2/H_2	**NiMo-NH_3/H_2**	**NiMo-NH_3**	**$NiMoO_4$**
C_{dl} (mF cm^{-2})	3.2	3.0	2.4	1.3
ECSA	20	18.8	15	8.1

Table S2. The XPS data of NiMo-based materials. The results were calculated from specific peak areas of XPS spectra.

Catalysts	**XPS data**		
	Ni^0/Ni^{2+}	Mo^0/Mo^{4+}	N (%)
NiMo-N_2/H_2	0.25	0.52	0
NiMo-NH_3/H_2	0.22	0.43	9.8
NiMo-NH_3	0.18	0.40	10.2

Table S3. The element contents of Fe-NiMo catalyst after OER activation.

Catalysts	**EDS(%)**				
	Ni	Mo	Fe	N	O
Fe-NiMo-N_2/H_2	35.7	4.8	20.0	0	39.5
Fe-NiMo-NH_3/H_2	40.8	1.4	18.9	1.8	37.1
Fe-NiMo-NH_3	38.5	1.9	19.2	2.1	38.3

Table S4. The comparison of the HER performance of NiMo-based catalysts with other state-of-the-art electrocatalysts in alkaline medium.

Catalysts	η@10 mA cm^{-2}	Tafel slope ($mV\ dec^{-1}$)	Substrate	Electrolyte	References
NiMo-NH_3/H_2	11	35	NF	1.0 KOH	This work
NiMo-N_2/H_2	27	47	NF	1.0 KOH	
NiMo-NH_3	29	68	NF	1.0 KOH	
$MoNi_4/MoO_2$@Ni	15	30	NF	1.0 KOH	[1]
Ni_4Mo/MoO_x	16	64	Cu foil	1.0 KOH	[2]
NiMo alloy	17	43	Ti foil	1.0 KOH	[3]
$MoS_2/CoNi_2S_4$	81	67	CFP	1.0 KOH	[4]
Nanoporous Co_2P	60	40	CFP	1.0 KOH	[5]
Co@Co_3O_4 nanosheet/Ni foam	90	44	NF	1.0 KOH	[6]
MoS_2/NiCo-LDH	78	76	CFP	1.0 KOH	[7]
$NiPt_3$@NiS	12	24	FTO	1.0 KOH	[8]
MoNi-HS	38	31	GCE	1.0 KOH	[9]
$Cu_{53}Ru_{47}$	15	30	GCE	1.0 KOH	[10]
Ni/WC@NC	77	68	GCE	1.0 KOH	[11]
Ni_3N/Ni	12	29	NF	1.0 KOH	[12]
Ni_3FeN	75	98	NF	1.0 KOH	[13]
Ni_2P/Fe_2P	121	67	GCE	1.0 KOH	[14]
Ni_3N_{1-x}	55	54	NF	1.0 KOH	[15]

Table S5. The comparison of the OER performance of Fe-NiMo-based catalysts with other state-of-the-art electrocatalysts in alkaline medium.

Catalysts	η_{10} (mV)	η_{100} (mV)	Tafel slope (mV dec^{-1})	Electrodes	References
Fe-NiMo-NH_3/H_2	192	219	28	NF	This work
Fe-NiMo-N_2/H_2	200	230	29	NF	
Fe-NiMo-NH_3	198	226	28	NF	
NF-AC-NiO_x-Fe	215	248	34.0	NF	[16]
Ni:FeOOH	214	270	36.2	NGF	[17]
Fe-doped β-$Ni(OH)_2$	219	280	53.0	NF	[18]
$NiFe(OH)_x/FeS$	/	255	/	IF	[19]
a-LNF(t-d)	189	310	36	glassy carbon	[20]
NiTe/NiS	/	257	49	NF	[21]
fcc-NiFe@NC	226	263	41	CC	[22]
$Ni_{0.8}Fe_{0.2}$-AHNA	190	248	34.7	NF	[23]
FeOOH(Se)	/	310	54	IF	[24]
$NiFeO_x$	230	271	31.5	CFP	[25]
DR-Ni_3FeN/N-G	250	310	38.0	RDE	[26]
$Ni_{60}Fe_{30}Mn_{10}$	208	270	62.0	Alloy Foam	[27]
NiFe hydroxides	245	280	28.0	NF	[28]
HG-$NiFe_x$	310	380	39	GCE	[29]
Ni-Fe LDH hollow prisms	280	370	49.4	GC	[30]
NiFe-OH-F-SR	-[a]	228	22.6	NF	[31]
EG/$Co_{0.85}Se$/NiFe LDH	203	260	57	Graphene Foam	[32]

Table S6. The comparison of the performance of MEAs employing noble or non-noble metal-based catalysts in alkaline medium.

Catalysts		**Electrode**	**Membrane**	**Efficiency Catalyst @1A/cm^2**	**Voltage @ *J* (V @ mA cm^{-2})**	**Temperature (^{o}C)**	**Ref.**
Anode catalyst	**Cathode catalyst**						
$NiMo-NH_3/H_2$	$Fe-NiMo-NH_3/H_2$	NF	Sustainion X37-50	75.1	1.57@1.0	80	**This work**
$NiMo-N_2/H_2$	$Fe-NiMo-N_2/H_2$	NF	Sustainion X37-50	70.3	1.68@1.0	80	
$NiMo-NH_3$	$Fe-NiMo-NH_3$	NF	Sustainion X37-50	72.6	1.62@1.0	80	
NiFe-LDH	Pt/C	CP	Sustainion X37-50	74.3	1.59@1.0	80	[33]
NiFe-LDH	Pt/C	CP	Sustainion X37-50	71.8	1.67@1.0	60	
IrO_x	Pt/C	CP	Sustainion X37-50	71.8	1.67@1.0	60	
IrO_x	Pt /C	carbon	FAA-3-50	/	1.8@1.15	70	[34]
IrO_2	Pt black	Ti form	A-201, Tokuyama	/	1.8@0.4	50	[35]
$NiFe_2O_4$	NiFeCo	Baekart	Sustainion X37-50	63.1	1.9@1.0	60	[36]
IrO_2	Pt	CP	Sustainion X37-50	73.6	1.63@1.0	60	
Ni	Ni	CP	A-201, Tokuyama	/	1.9@0.15	50	[37]
IrO_2	Pt/C	NF/CP	SEBS-Pi	/	2.0@0.4	50	[38]
$CuCoO_3$	$Ni/(CeO_2-La_2O_3)/C$	CP/CC	A-201, Tokuyama	/	1.9@0.47	50	[39]
$Cu_{0.81}Co_{2.19}O_4$	Pt/C	NF	Fumasep FAA-3-PE-30	/	1.68@0.1	30	[40]
$Cu_{0.7}Co_{2.3}O_4$	Pt/C	stainless steel meshes	Membrane with quaternary ammonium function groups	68.3	1.8@1.0	25	[41]
Co_3O_4				/	1.8@0.6	25	

References

(1) Zhang, J.; Wang, T.; Liu, P.; Liao, Z.; Liu, S.; Zhuang, X.; Chen, M.; Zschech, E.; Feng, X. *Nat. Commun.* **2017**, *8*, 15437.

(2) An, Y.; Long, X.; Ma, M.; Hu, J.; Lin, H.; Zhou, D.; Xing, Z.; Huang, B.; Yang, S. *Adv. Energy Mater.* **2019**, *9*, 1901454.

(3) Nairan, A.; Zou, P.; Liang, C.; Liu, J.; Wu, D.; Liu, P.; Yang, C. *Adv. Funct. Mater.* **2019**, *29*, 1903747.

(4) Hu, J.; Zhang, C.; Yang, P.; Xiao, J.; Deng, T.; Liu, Z.; Huang, B.; Leung, M. K. H.; Yang, S. *Adv. Funct. Mater.* **2020**, *30*, 1908520.

(5) Tan, Y.; Wang, H.; Liu, P.; Cheng, C.; Zhu, F.; Hirata, A.; Chen, M. *Adv. Mater.* **2016**, *28*, 2951–2955.

(6) Yan, X.; Tian, L.; He, M.; Chen, X. *Nano Lett.* **2015**, *15*, 6015–6021.

(7) Hu, J.; Zhang, C.; Jiang, L.; Lin, H.; An, Y.; Zhou, D.; Leung, M. K. H.; Yang, S. *Joule* **2017**, *1*, 383–393.

(8) Panda, C.; Menezes, P. W.; Yao, S.; Schmidt, J.; Walter, C.; Hausmann, J. N.; Driess, M. *J. Am. Chem. Soc.* **2019**, *141*, 13306–13310.

(9) Zhou, Y.; Luo, M.; Zhang, W.; Zhang, Z.; Meng, X.; Shen, X.; Liu, H.; Zhou, M.; Zeng, X. *ACS Appl. Mater. Interfaces* **2019**, *11*, 21998–22004.

(10) Wu, Q.; Luo, M.; Han, J.; Peng, W.; Zhao, Y.; Chen, D.; Peng, M.; Liu, J.; de Groot, F. M. F.; Tan, Y. *ACS Energy Lett.* **2020**, *5*, 192–199.

(11) Ma, Y.-Y.; Lang, Z.-L.; Yan, L.-K.; Wang, Y.-H.; Tan, H.-Q.; Feng, K.; Xia, Y.-J.; Zhong, J.; Liu, Y.; Kang, Z.-H.; et al. *Energy Environ. Sci.* **2018**, *11*, 2114–2123.

(12) Song, F.; Li, W.; Yang, J.; Han, G.; Liao, P.; Sun, Y. *Nat. Commun.* **2018**, *9*, 4531.

(13) Zhang, B.; Xiao, C.; Xie, S.; Liang, J.; Chen, X.; Tang, Y. *Chem. Mater.* **2016**, *28*, 6934–6941.

(14) Ge, Y.; Dong, P.; Craig, S. R.; Ajayan, P. M.; Ye, M.; Shen, J. *Adv. Energy Mater.* **2018**, *8*, 1800484.

(15) Liu, B.; He, B.; Peng, H.-Q.; Zhao, Y.; Cheng, J.; Xia, J.; Shen, J.; Ng, T.-W.; Meng, X.; Lee, C.-S.; et al. *Adv. Sci.* **2018**, *5*, 1800406.

(16) Song, F.; Busch, M. M.; Lassalle-Kaiser, B.; Hsu, C.-S.; Petkucheva, E.; Bensimon, M.; Chen, H. M.; Corminboeuf, C.; Hu, X. *ACS Cent. Sci.* **2019**, *5*, 558–568.

(17) Suryawanshi, M. P.; Ghorpade, U. V; Shin, S. W.; Suryawanshi, U. P.; Jo, E.; Kim, J. H. *ACS Catal.* **2019**, *9*, 5025–5034.

(18) Kou, T.; Wang, S.; Hauser, J. L.; Chen, M.; Oliver, S. R. J.; Ye, Y.; Guo, J.; Li, Y. *ACS Energy Lett.* **2019**, *4*, 622–628.

(19) Niu, S.; Jiang, W.-J.; Tang, T.; Yuan, L.-P.; Luo, H.; Hu, J.-S. *Adv. Funct. Mater.* **2019**, *29*, 1902180.

(20) Chen, G.; Zhu, Y.; Chen, H. M.; Hu, Z.; Hung, S.-F.; Ma, N.; Dai, J.; Lin, H.-J.; Chen, C.-T.; Zhou, W.; et al. *Adv. Mater.* **2019**, *31*, 1900883.

(21) Xue, Z.; Li, X.; Liu, Q.; Cai, M.; Liu, K.; Liu, M.; Ke, Z.; Liu, X.; Li, G. *Adv. Mater.* **2019**, *31*, 1900430.

(22) Wang, C.; Yang, H.; Zhang, Y.; Wang, Q. *Angew. Chemie Int. Ed.* **2019**, *58*, 6099–6103.

(23) Liang, C.; Zou, P.; Nairan, A.; Zhang, Y.; Liu, J.; Liu, K.; Hu, S.; Kang, F.; Fan, H. J.; Yang, C. *Energy Environ. Sci.* **2020**, *13*, 86–95.

(24) Niu, S.; Jiang, W.-J.; Wei, Z.; Tang, T.; Ma, J.; Hu, J.-S.; Wan, L.-J. *J. Am. Chem. Soc.* **2019**, *141*, 7005–7013.

(25) Wang, H.; Lee, H.-W.; Deng, Y.; Lu, Z.; Hsu, P.-C.; Liu, Y.; Lin, D.; Cui, Y. *Nat. Commun.* **2015**, *6*, 7261.

(26) Zhao, S.; Li, M.; Han, M.; Xu, D.; Yang, J.; Lin, Y.; Shi, N.-E.; Lu, Y.; Yang, R.; Liu, B.; et al. *Adv. Funct. Mater.* **2018**, *28*, 1706018.

(27) Detsi, E.; Cook, J. B.; Lesel, B. K.; Turner, C. L.; Liang, Y.-L.; Robbennolt, S.; Tolbert, S. H. *Energy Environ. Sci.* **2016**, *9*, 540–549.

(28) Senthil, R. A.; Pan, J.; Yang, X.; Sun, Y. *Int. J. Hydrogen Energy* **2018**, *43*, 21824–21834.

(29) Wang, J.; Gan, L.; Zhang, W.; Peng, Y.; Yu, H.; Yan, Q.; Xia, X.; Wang, X. *Sci. Adv.* **2018**, *4*, eaap7970.

(30) Yu, L.; Yang, J. F.; Guan, B. Y.; Lu, Y.; Lou, X. W. D. *Angewandte Chemie - International Edition*. 2018, pp 172–176.

(31) Zhang, B.; Jiang, K.; Wang, H.; Hu, S. *Nano Lett.* **2019**, *19*, 530–537.

(32) Hou, Y.; Lohe, M. R.; Zhang, J.; Liu, S.; Zhuang, X.; Feng, X. *Energy Environ. Sci.* **2016**, *9*, 478–483.

(33) Koshikawa, H.; Murase, H.; Hayashi, T.; Nakajima, K.; Mashiko, H.; Shiraishi, S.; Tsuji, Y. *ACS Catal.* **2020**, *10*, 1886–1893.

(34) Park, J. E.; Kang, S. Y.; Oh, S.-H.; Kim, J. K.; Lim, M. S.; Ahn, C.-Y.; Cho, Y.-H.; Sung, Y.-E. *Electrochim. Acta* **2019**, *295*, 99–106.

(35) Leng, Y.; Chen, G.; Mendoza, A. J.; Tighe, T. B.; Hickner, M. A.; Wang, C.-Y. *J. Am. Chem. Soc.* **2012**, *134*, 9054–9057.

(36) Kaczur, J. J.; Yang, H.; Liu, Z.; Sajjad, S. D.; Masel, R. I. *Frontiers in Chemistry* . 2018, p 263.

(37) Ahn, S. H.; Lee, B.-S.; Choi, I.; Yoo, S. J.; Kim, H.-J.; Cho, E.; Henkensmeier, D.; Nam, S. W.; Kim, S.-K.; Jang, J. H. *Appl. Catal. B Environ.* **2014**, *154–155*, 197–205.

(38) Su, X.; Gao, L.; Hu, L.; Qaisrani, N. A.; Yan, X.; Zhang, W.; Jiang, X.; Ruan, X.; He, G. *J. Memb. Sci.* **2019**, *581*, 283–292.

(39) Pavel, C. C.; Cecconi, F.; Emiliani, C.; Santiccioli, S.; Scaffidi, A.; Catanorchi, S.; Comotti, M. *Angew. Chemie Int. Ed.* **2014**, *53*, 1378–1381.

(40) Choi, W.-S.; Jang, M. J.; Park, Y. S.; Lee, K. H.; Lee, J. Y.; Seo, M.-H.; Choi, S. M. *ACS Appl. Mater. Interfaces* **2018**, *10*, 38663–38668.

(41) Wu, X.; Scott, K. *J. Mater. Chem.* **2011**, *21*, 12344–12351.